REPORT

GALAXIES

A massive stellar bulge in a regularly rotating galaxy 1.2 billion years after the Big Bang

Federico Lelli[1,2]*, Enrico M. Di Teodoro[3], Filippo Fraternali[4], Allison W. S. Man[5], Zhi-Yu Zhang[6], Carlos De Breuck[7], Timothy A. Davis[1], Roberto Maiolino[8,9]

Cosmological models predict that galaxies forming in the early Universe experience a chaotic phase of gas accretion and star formation, followed by gas ejection due to feedback processes. Galaxy bulges may assemble later via mergers or internal evolution. Here we present submillimeter observations (with spatial resolution of 700 parsecs) of ALESS 073.1, a starburst galaxy at redshift $z \simeq 5$ when the Universe was 1.2 billion years old. This galaxy's cold gas forms a regularly rotating disk with negligible noncircular motions. The galaxy rotation curve requires the presence of a central bulge in addition to a star-forming disk. We conclude that massive bulges and regularly rotating disks can form more rapidly in the early Universe than predicted by models of galaxy formation.

In the standard Lambda cold dark matter (ΛCDM) cosmological model, galaxies form inside dark matter (DM) halos when primordial gas cools, collapses, and begins star formation (*1*). At early times, when the Universe was only 10% of its current age (redshift $z \simeq 5$), ΛCDM models predict that galaxies undergo a turbulent phase of gas accretion from the cosmic web, leading to violent bursts of star formation and black hole growth (*2*). These are rapidly followed by massive gas outflows due to feedback from supernovae and active galactic nuclei (AGN). Strong stellar and AGN feedback are needed in ΛCDM models to reproduce the observed number of galaxies per unit volume per unit mass (the galaxy stellar mass function) and to quench star formation in the most massive DM halos, reproducing the observed population of quiescent early-type galaxies at $z = 0$ (*3*). In the hierarchical ΛCDM scenario, galaxy bulges (the spheroidal stellar components in the central parts of massive galaxies) are expected to form either after the merger of two galaxies of similar mass or via secular dynamical processes within the stellar disk (*4*). Observation of galaxies at high redshifts enables us to test these scenarios by searching for these physical processes in action.

The 158-μm emission line of singly ionized carbon, [C II], is a major coolant of the interstellar medium of galaxies and traces a combination of atomic and molecular hydrogen phases. The [C II] line has been observed up to $z \simeq 7.5$ (*5*), and several rotating disks have been identified at $z > 3$ (*6*–*8*). Most existing observations only marginally resolve the [C II] distribution and kinematics, and thus cannot distinguish between rotating disks, galaxy mergers, or gas inflows and outflows. Limited spatial resolution has prevented the measurement of well-sampled rotation curves (with more than six independent elements), which could be used to measure different mass components by fitting dynamical models.

[1]School of Physics and Astronomy, Cardiff University, Cardiff CF24 3AA, UK. [2]Arcetri Astrophysical Observatory, Istituto Nazionale di Astrofisica, Florence 50125, Italy. [3]Department of Physics & Astronomy, Johns Hopkins University, Baltimore, MD 21218, USA. [4]Kapteyn Astronomical Institute, University of Groningen, Groningen 9700 AV, Netherlands. [5]Dunlap Institute for Astronomy & Astrophysics, University of Toronto, Toronto, ON M5S 3H4, Canada. [6]School of Astronomy and Space Science, Nanjing University, Nanjing 210023, P. R. China. [7]European Southern Observatory, Garching bei München 85748, Germany. [8]Kavli Institute for Cosmology, University of Cambridge, Cambridge CB3 0HA, UK. [9]Cavendish Laboratory, University of Cambridge, Cambridge CB3 0HE, UK.
*Corresponding author. Email: federico.lelli@inaf.it

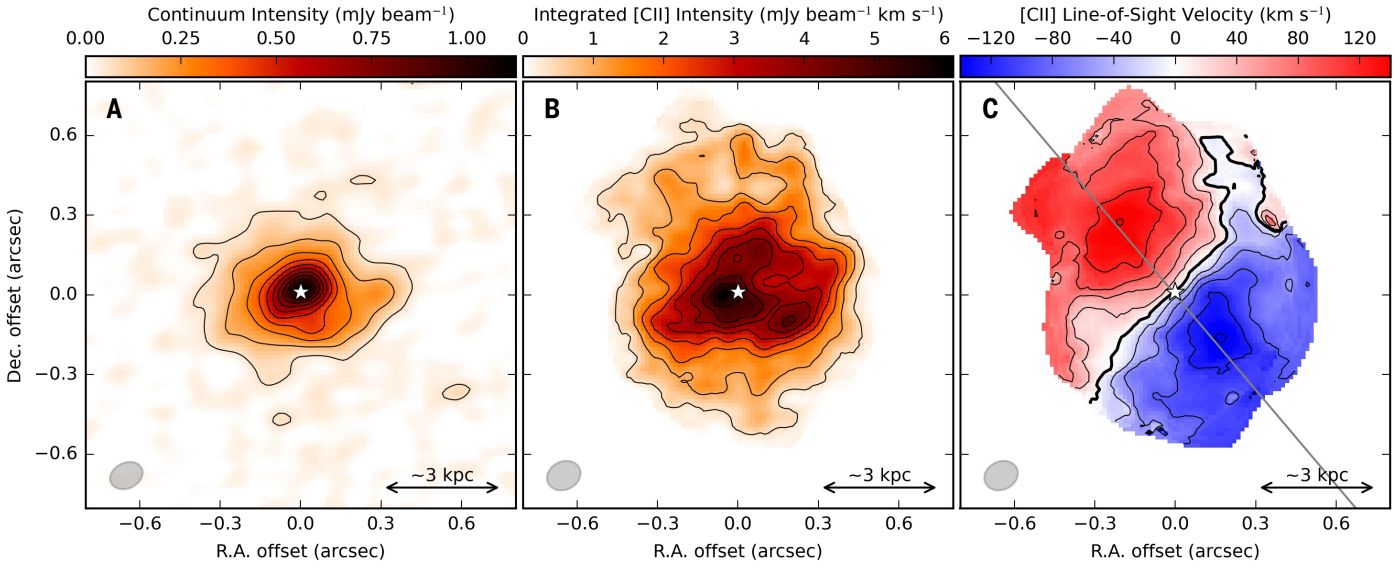

Fig. 1. ALMA observations of ALESS 073.1. (**A**) Continuum emission at 160 μm (rest-frame) tracing dust heated by young stars, (**B**) [C II] intensity map tracing cold gas, and (**C**) [C II] velocity field showing a rotating disk. North is up; east is left. The kinematic center, located at right ascension (R.A.) $03^h\ 32^m\ 29.295^s$ and declination (Dec.) −27°56′19.″60, is represented by a white star. The beam size is plotted as the gray ellipse in the bottom-left corner. The physical scale is indicated by the scale bar in the bottom-right corner. In (A), iso-emission contours range from 0.055 to 1 mJy beam^{-1} (where 1 mJy = 10^{-29} W m^{-2} Hz^{-1}) in steps of 0.11 mJy beam^{-1}. In (B), iso-emission contours range from 0.35 to 6 mJy beam^{-1} km s^{-1} in steps of 0.7 mJy beam^{-1} km s^{-1}. In (A) and (B), the lowest iso-emission contour corresponds to a signal-to-noise ratio of ~3. In (C), iso-velocity contours range from −120 to +120 km s^{-1} in steps of 30 km s^{-1}, the bold contour indicates the systemic velocity (set to zero), and the gray line shows the kinematic major axis.

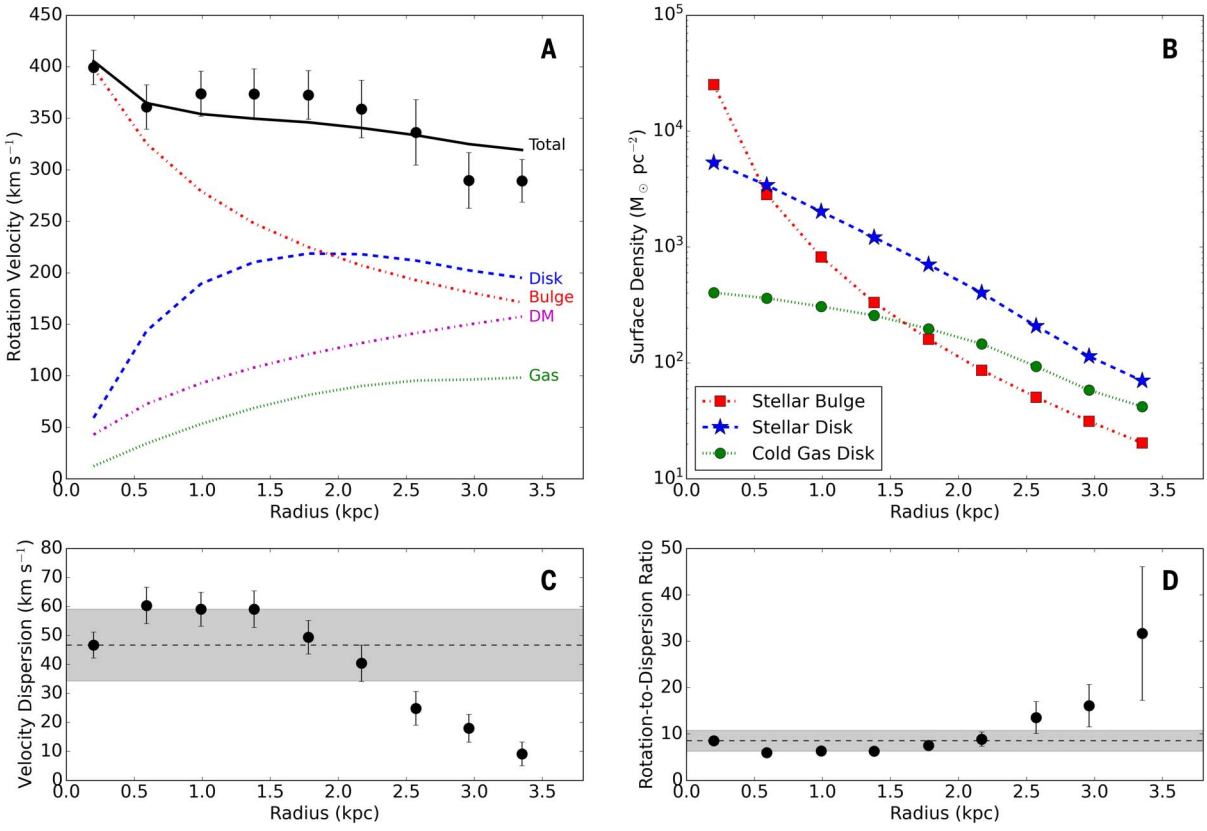

Fig. 2. Mass model of ALESS 073.1. (**A**) The observed rotation curve (black circles) adopting the best-fitting inclination angle of 22°. The model rotation curve (black solid line) is the total of contributions from the stellar bulge (red dot-dashed line), stellar disk (blue dashed line), cold gas disk (green dotted line), and DM halo (magenta dash-dotted line). (**B**) Surface density profiles of the bulge (red squares), stellar disk (blue stars), and cold gas disk (green circles) adopting the best-fitting masses (*9*). The bulge profile assumes a de Vaucouleurs' distribution (*30*). The stellar and gas disk profiles are obtained from azimuthal averages of the dust continuum and [C II] intensity maps, respectively. The uncertainties on these profiles are dominated by the systematic uncertainty on the normalizing masses (*9*). (**C**) [C II] velocity dispersion profile. (**D**) Disk rotational support as a function of radius. In (C) and (D), the dashed line and gray band show the median value and median absolute deviation, respectively. In (A), (C), and (D), the error bars show ±1σ uncertainties (*9*).

We used the Atacama Large Millimeter/submillimeter Array (ALMA) to observe a star-forming galaxy at z = 4.75 (*6*) at a spatial resolution of ~0.″11, corresponding to 0.7 kpc in a ΛCDM cosmology (*9*). The target, ALESS 073.1 (LESS J033229.3-275619), is a strong submillimeter source (*10*). Its large far-infrared luminosity suggests an ongoing starburst with an estimated star-formation rate of ~1000 solar masses ($M_\odot$) per year (*10*, *11*). ALESS 073.1 contains a dust-obscured AGN (*12*). These extreme properties indicate that the galaxy may drive a massive gas outflow (*11*). Previous [C II] observations with ALMA indicated a possible rotating disk (*6*), but the spatial resolution (0.″5, corresponding to ~3 kpc) was insufficient to determine its detailed properties or identify gas inflows and outflows.

Figure 1A shows the continuum map at rest-frame 160 μm, which traces dust heated by the star-formation activity. Figure 1B shows the integrated [C II] intensity map, which traces the cold gas distribution. The [C II] emission is about twice as extended as the dust emission and shows an asymmetry to the northeast. Similar lopsided gas disks are common in the nearby Universe, forming nearly half of the local population of atomic gas disks (*13*).

The [C II] velocity field (moment one map; Fig. 1C) shows a regularly rotating disk. Rotating disks and galaxy mergers can be difficult to distinguish when observed at low spatial resolutions (*14*). This is not the case for ALESS 073.1 because the area with detectable [C II] emission is covered by ~45 resolution elements. The kinematic major axis is perpendicular to the kinematic minor axis, implying that non-circular motions are negligible in the inner parts of the gas disk (*15*). The gas kinematics are less regular in the northeastern extension: This may be due to recently accreted gas, a warped outer disk, or streaming motions along a spiral arm (*9*). The limited signal-to-noise ratio in the outer regions does not allow us to distinguish between these possibilities. Overall, the kinematic regularity of the [C II] disk is unexpected for a starburst AGN-host galaxy at $z \simeq 0$.

We model the [C II] kinematics using the software ^{3D}BAROLO (*16*), which fits the observational data with a rotating disk model (*9*). This determines the [C II] surface brightness profile, the rotation curve, and the intrinsic velocity dispersion profile. The best-fitting rotation curve (Fig. 2A) rises steeply in the central parts and declines across the disk. Similar rotation curves are observed in bulge-dominated disk galaxies in the nearby Universe (*17*–*19*), so there might be a bulge component in ALESS 073.1. The normalization of the rotation curve depends on the disk inclination, which we treat as a free parameter below.

We use the derived rotation curve to constrain the mass distribution within the galaxy. Our fiducial mass model has four components: cold gas disk, stellar disk, stellar bulge, and DM halo. We also investigate mass models with three components, which we find either cannot fit the observations or are less plausible in the ΛCDM paradigm (*9*). We assume that the [C II] density profile traces the distribution of the cold gas disk, whereas the dust density profile traces the distribution of the stellar disk (Fig. 2B), because dust absorbs ultraviolet radiation from young stars and reemits it at

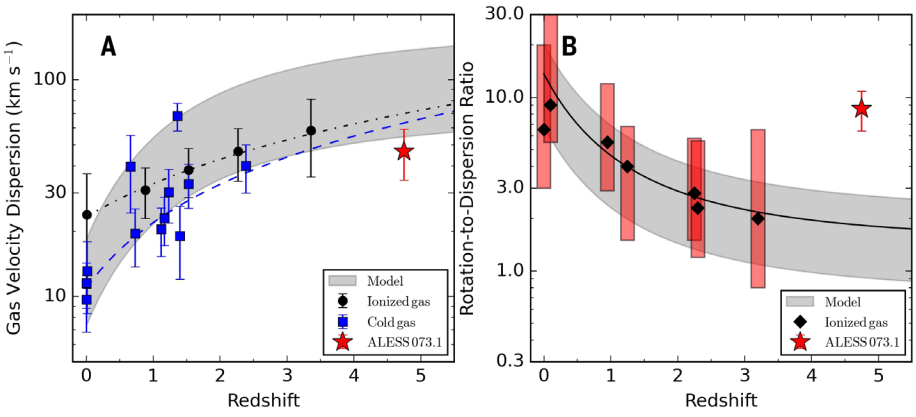

Fig. 3. Turbulence and rotational support of galaxies as a function of cosmic time. (**A**) Gas velocity dispersion and (**B**) V_{rot}/σ_V versus redshift. Gray bands show a semi-empirical model based on Toomre's disk instability parameter (*21*). In (A), the black dot-dashed line and the blue dashed line show the velocity dispersion evolution inferred from warm ionized gas data (black circles; averages from galaxy samples) and cold neutral gas data (blue squares; averages for $z = 0$ and individual galaxies for $z > 0.5$), respectively (*24*). In (B), black diamonds and red bars show, respectively, the median and 90% distribution of ionized gas surveys (*21*). The red star represents ALESS 073.1. Error bars correspond to ±1σ uncertainties.

far-infrared wavelengths. The two additional components (bulge and DM halo) are modeled with analytic functions (*9*). The bulge component implicitly includes the contribution of the central supermassive black hole, which contributes <10% of the central mass in high-z galaxies (*8*).

For the best-fitting inclination angle of 22°, the [C II] disk rotates at velocities (V_{rot}) of 300 to 400 km s^{-1} (Fig. 2A). Similar rotational speeds are observed in the most massive early-type galaxies at $z = 0$ that host molecular gas disks (*20*), so we conclude that they are the likely descendants of galaxies similar to ALESS 073.1. The intrinsic velocity dispersion (σ_V) reaches 50 to 60 km s^{-1} at small radii and decreases to ~10 km s^{-1} in the outer parts (Fig. 2C). The ratio of rotation velocity to velocity dispersion (Fig. 2D) is ~10 within 2.5 kpc, similar to that of cold gas disks at $z = 0$ (*21*). The [C II] disk of ALESS 073.1 is supported by rotation, not turbulence.

The bulge component of the model is necessary to reproduce the observed high rotation speeds at small radii. We obtain a bulge–to–total mass ratio $M_{bul}/M_{baryon} = 0.44$, where M_{baryon} is given by the sum of all baryonic (non-DM) components within 3.5 kpc. This ratio is nearly independent of the disk inclination because it is largely driven by the shapes of the observed rotation curve and of the baryonic gravitational contributions, not by their absolute normalizations. Baryons dominate the gravitational potential within 3.5 kpc, similar to massive galaxies at $z = 0$ (*19*) and $z = 1$ to 3 (*22*, *23*). In ΛCDM cosmology, DM halos are expected to have low concentrations at high z, whereas baryons can efficiently cool and collapse to the bottom of the potential well, reaching high concentrations. Thus, DM halos become gravitationally dominant at large radii.

Gas disks in the early Universe are expected to be more turbulent than their local analogs: the gas velocity dispersion is thought to increase with redshift, whereas the degree of rotational support (V_{rot}/σ_V) decreases (*21*, *24*). The enhanced turbulence may be driven by gravitational instabilities from cold gas flows, and/or by stellar and AGN feedback (*25*). At $z \geq 1$, however, the limited spatial resolution can bias the measurements of V_{rot} and σ_V (beam-smearing effects), leading to systematic overestimates of σ_V and underestimates of V_{rot}/σ_V (*26*). The gas velocity dispersion of ALESS 073.1 is consistent with the extrapolations from data at $z < 3.5$ (Fig. 3A) but lies at the low σ_V boundary of the prediction of a semi-empirical model based on Toomre's disk instability parameter (*21*), despite the galaxy hosting a starburst and a dust-obscured AGN. The rotational support of the gas disk of ALESS 073.1 is much higher than the value predicted by the same model (Fig. 3B), which has been used to describe kinematic measurements at $z < 3.5$ (*21*). The V_{rot}/σ_V ratio is similar to that of gas disks in the local Universe (Fig. 3B). This suggests that both starburst and AGN feedback have only a gentle effect on the cold interstellar medium of ALESS 073.1 because the [C II] disk is regular and unperturbed, contrary to galaxy formation models with violent feedback.

It remains unknown whether bulges exist in the early Universe ($z > 4$), given the lack of high-resolution infrared observations probing the stellar mass distribution. In ALESS 073.1, we use the gas kinematics to infer the presence of a central massive component that is not traced by the dust. This is likely a stellar bulge hosting a supermassive black hole. Bulges form either from the secular evolution of stellar disks or after major galaxy mergers (*4*). Both mechanisms could be at play in ALESS 073.1, but they must act on short time scales because the Universe was only 1.2 billion years old at $z \simeq 4.75$. Any major merger must have happened at even earlier cosmic epochs to provide time for the gas kinematics to relax to regular rotation. The orbital time at the last measured point of the rotation curve is about 5×10^7 years, and about five revolutions may be required to relax the disk, so any major merger must have happened at $z > 5.5$. ALMA observations of a quasar-host galaxy at $z \simeq 6.6$ with similar spatial resolution show that the [C II] kinematics can be heavily disturbed at this younger epoch (~0.8 billion years after the Big Bang), possibly owing to mergers or interactions (*27*). Bulges may also develop from star formation inside AGN-driven gas outflows (*28*, *29*), which could occur on short time scales. Although we observe only a single object, we conclude that the Universe produced regularly rotating galaxy disks with prominent bulges at <10% of its current age. This implies that the formation of massive galaxies and their central bulges must be a fast and efficient process.

REFERENCES AND NOTES

1. S. D. M. White, M. J. Rees, *Mon. Not. R. Astron. Soc.* **183**, 341–358 (1978).
2. A. Dekel, Y. Birnboim, *Mon. Not. R. Astron. Soc.* **368**, 2–20 (2006).
3. M. Vogelsberger *et al.*, *Nature* **509**, 177–182 (2014).
4. J. Kormendy, R. C. Kennicutt Jr., *Annu. Rev. Astron. Astrophys.* **42**, 603–683 (2004).
5. E. Bañados *et al.*, *Astrophys. J.* **881**, L23 (2019).
6. C. De Breuck *et al.*, *Astron. Astrophys.* **565**, A59 (2014).
7. G. C. Jones *et al.*, *Astrophys. J.* **850**, 180 (2017).
8. A. Pensabene *et al.*, *Astron. Astrophys.* **637**, A84 (2020).
9. Materials and methods are available as supplementary materials.
10. K. E. K. Coppin *et al.*, *Mon. Not. R. Astron. Soc.* **395**, 1905–1914 (2009).
11. R. Gilli *et al.*, *Astron. Astrophys.* **562**, A67 (2014).
12. R. Gilli *et al.*, *Astrophys. J.* **730**, L28 (2011).
13. R. Sancisi, F. Fraternali, T. Oosterloo, T. van der Hulst, *Astron. Astrophys. Rev.* **15**, 189–223 (2008).
14. S. M. Sweet *et al.*, *Mon. Not. R. Astron. Soc.* **485**, 5700–5714 (2019).
15. F. Fraternali, T. Oosterloo, R. Sancisi, G. van Moorsel, *Astrophys. J.* **562**, L47–L50 (2001).
16. E. M. Di Teodoro, F. Fraternali, *Mon. Not. R. Astron. Soc.* **451**, 3021–3033 (2015).
17. S. Casertano, J. H. van Gorkom, *Astron. J.* **101**, 1231 (1991).
18. E. Noordermeer, J. M. van der Hulst, R. Sancisi, R. S. Swaters, T. S. van Albada, *Mon. Not. R. Astron. Soc.* **376**, 1513–1546 (2007).
19. F. Lelli, S. S. McGaugh, J. M. Schombert, *Astron. J.* **152**, 157 (2016).
20. T. A. Davis *et al.*, *Mon. Not. R. Astron. Soc.* **455**, 214–226 (2016).
21. E. Wisnioski *et al.*, *Astrophys. J.* **799**, 209 (2015).
22. F. Lelli *et al.*, *Mon. Not. R. Astron. Soc.* **479**, 5440–5447 (2018).
23. R. Genzel *et al.*, *Nature* **543**, 397–401 (2017).
24. H. Übler *et al.*, *Astrophys. J.* **880**, 48 (2019).
25. M. D. Lehnert *et al.*, *Astrophys. J.* **699**, 1660–1678 (2009).
26. E. M. Di Teodoro, F. Fraternali, S. H. Miller, *Astron. Astrophys.* **594**, A77 (2016).
27. B. P. Venemans *et al.*, *Astrophys. J.* **874**, L30 (2019).

28. W. Ishibashi, A. C. Fabian, *Mon. Not. R. Astron. Soc.* **441**, 1474–1478 (2014).
29. R. Maiolino *et al*., *Nature* **544**, 202–206 (2017).
30. G. de Vaucouleurs, *Ann. d'Astrophys.* **11**, 247 (1948).

ACKNOWLEDGMENTS

We thank L. Legrand and H. Übler for providing tabular data from their publications. F.L. thanks P. Li for technical support with the Markov Chain Monte Carlo fitting code. ALMA is a partnership of ESO (representing its member states), NSF (USA), and NINS (Japan), together with NRC (Canada), MOST and ASIAA (Taiwan), and KASI (Republic of Korea), in cooperation with the Republic of Chile. The Joint ALMA Observatory is operated by ESO, AUI/NRAO, and NAOJ. **Funding:** F.L. was supported by an ESO fellowship during the initial stages of this project. E.M.D.T. was supported by the U.S. National Science Foundation under grant 1616177. F.F. acknowledges support from the Friedrich Wilhelm Bessel Research Award Programme of the Alexander von Humboldt Foundation. A.W.S.M. is supported by a Dunlap Fellowship at the Dunlap Institute for Astronomy & Astrophysics, funded through an endowment established by the David Dunlap family and the University of Toronto. R.M. acknowledges ERC Advanced Grant 695671 "QUENCH" and support from the Science and Technology Facilities Council (STFC). **Author contributions:** F.L.: conceptualization, data curation, formal analysis, investigation, methodology, project administration, software, validation, visualization, writing – original draft. E.M.D.T.: conceptualization, formal analysis, methodology, software, visualization, writing – review & editing. F.F.: conceptualization, methodology, software, writing – review & editing. A.W.S.M.: formal analysis, writing – review & editing. Z.-Y.Z.: formal analysis, writing – review & editing. C.D.B.: data curation, writing – review & editing. T.A.D.: resources, writing – review & editing. R.M.: resources, writing – review & editing. **Competing interests:** We have no competing interests. **Data and materials availability:** The ALMA data are available at https://almascience.eso.org/asax/ under project codes ADS/JAO. ALMA 2017.1.01471.S, 2015.1.00456.S, and 2011.0.00124.S. The Hubble Space Telescope data are available at https://archive.stsci.edu/hst/ (proposal ID 12061, dataset ibeuglqlq). Supplementary data files contain the observed [C II] data cube (data S1), the [C II] moment maps (data S2 and S3), the model outputs from ^{3D}BAROLO (data S4 to S6), the model outputs from GALFIT (data S7), and the best-fitting mass model (data S8).

SUPPLEMENTARY MATERIALS

science.sciencemag.org/content/371/6530/713/suppl/DC1
Materials and Methods
Figs. S1 to S6
Tables S1 and S2
References (*31*–*72*)
Data S1 to S8

10 April 2020; accepted 17 December 2020
10.1126/science.abc1893